Full Length Article

Enhancing the performance of a PtPd/HY catalyst for HDPE/VGO hydrocracking through zeolite desilication

Francisco J. Vela [a], Roberto Palos [a,b], Juan Rafael García [c], Ulises Sedran [c], Javier Bilbao [a], José M. Arandes [a], Alazne Gutiérrez [a,*]

[a] *Department of Chemical Engineering, University of the Basque Country UPV/EHU, PO Box 644, 48080 Bilbao, Spain*
[b] *Department of Chemical and Environmental Engineering, University of the Basque Country UPV/EHU, Plaza Ingeniero Torres Quevedo 1, 48013 Bilbao, Spain*
[c] *Instituto de Investigaciones en Catálisis y Petroquímica INCAPE (UNL–CONICET), Colectora Ruta Nac. N° 168 Km 0 – Paraje El Pozo, 3000 Santa Fe, Argentina*

A R T I C L E I N F O

A B S T R A C T

The valorization of post-consumer waste plastic in a refinery is an attractive initiative to avoid environmental problems caused by the poor plastic waste management. The modification of a bifunctional PtPd/HY catalyst through desilication (using NaOH) of the ultrastable HY zeolite has been carried out to upgrade waste plastic (high-density polyethylene (HDPE)) dissolved in a secondary refinery stream (vacuum gas oil (VGO)) through hydrocracking. Three different catalysts have been studied: the parent (Cat-A), undergoing a desilication cycle (Cat-B), and subjected to two cycles of desilication (Cat-C). The characterization techniques employed have been: N_2 adsorption–desorption, TEM, ICP-AES, *tert*-butylamine-TPD, pyridine FTIR, WDXRF, XRD and TPO. The hydrocracking tests have been carried out in a semi-batch reactor at: 440 °C; 80 bar; catalyst to feed ratio, 0.1 g_{cat} $(g_{feed})^{-1}$; HDPE to feed ratio, 0.2 g_{HDPE} $(g_{feed})^{-1}$; and reaction time, 2 h. The products have been fractioned according to their boiling point range in: gas, naphtha, light cycle oil, heavy cycle oil and coke. The composition of each fraction has been determined in terms of concentration of paraffins, olefins, naphthenes and (mono-, di- and poly-) aromatics. The results show that alkaline treated catalysts enhance the fuel production, with high HDPE and HCO conversions. The Cat-C (the one submitted to two desilication cycles) has displayed the greatest performance, reducing by half the gas yield and increasing the naphtha yield by 51 wt% respect to those obtained with the parent catalyst (Cat-A). Moreover, it has decreased the coke deposition and the coke formed has been less developed.

1. Introduction

Plastic pollution is one of the most significant environmental threats to the planet, since the rapidly increasing production of waste plastics overwhelms the ability to manage them [1]. Geyer et al.[2] estimated that more than 50 % of waste plastic discarded globally is not recycled and, consequently, between 4 and 12 million tons of plastic enter into the oceans every year [3]. It should be noted that society's concern about the management of waste plastics has increased with the knowledge of the adverse health effects of microplastics on the natural aqueous environment [4], soil environment [5] and in the atmosphere [6]. Furthermore, the SARS-CoV-2 pandemic has significantly increased society's awareness of the need of a proper waste management strategy on a massive scale [7].

For large-scale recycling of waste plastic, the most attractive

technologies are gasification [8] and pyrolysis [9,10]. The latter has acquired a remarkable level of technological development, with pilot and demonstration plant-scale units aimed at fuels production [11]. However, given the inherent difficulties for developing and establishing new industries for this purpose (need for heavy investments in fixed assets, obtaining fuel with an approved composition and its commercialization), Palos et al. [12] have proposed to valorize waste plastics in refinery units (Waste Refinery). Since plastics are produced with monomers obtained in the oil industry, it would be appropriate to involve oil refineries in their recovery and recycling, promoting the circular economy. This proposal will bring a significant decrease in oil consumption and will improve society's perception of refineries. Commercial units installed at refineries would be used for producing fuels, the composition of which could be adapted to the legal requirements using the existing separation and reforming units in the refineries. In

addition, the fuels could be marketed and distributed by the conventional means. The Waste Refinery is in line with other initiatives to intensify oil production, such as the intensification of the valorization of secondary refinery streams [13,14], biomass-derived streams [15–17] or shale oil [18].

Among the catalytic processes available in refineries, hydrocracking receives a great deal of attention for the valorization of waste plastic based on its versatility. Nonetheless, any progress in this initiative requires knowledge of the fundamental aspects of plastics hydrocracking and in particular the selection of the right catalyst and conditions. Industrial hydrocracking catalysts contain an acid support (such as zeolites), which is in charge of the cracking reactions, and metals (either transition or precious metals) that promote the hydrogenation activity. Besides, to obtain a pure bifunctional behavior, these functions must be well-balanced to provide an appropriate cracking/hydrogenation balance [19,20]. The composition of the catalysts has been tuned to maximize the formation of fractions with commercial interest, such as naphtha and diesel, from secondary refinery streams like VGO (vacuum gasoil) [21,22]. However, for hydrocracking neat plastics or plastics blended with secondary refinery streams it is necessary to develop new catalysts specifically designed for this purpose. Indeed, conventional hydrocracking catalysts produce excessive amounts of gas products, together with high contents of coke and low conversion of plastic [23–25]. Therefore, an aspect to be improved in these catalysts, especially in the zeolites used as supports, is that related to diffusion restrictions and their acidity, that causes an excessive overcracking and condensation to coke [26,27].

Strategies to modify zeolite properties include a post-treatment by desilication using an alkaline metal hydroxide or an organic hydroxide. This treatment results in the creation of a hierarchical structure since the formation of mesopores takes place. The presence of mesopores in the zeolite crystals favors the diffusion of the reactants, reaction intermediates and products, increasing the achieved conversion and attenuating deactivation by coke deposition [28]. Furthermore, the desilication treatment also changes the acidity of the zeolite decreasing the concentration of Brønsted acid sites but increasing that of Lewis acid sites [29]. In this way, the extent of undesirable reactions, such as aromatics condensation and hydrogen-transfer reactions, which are catalyzed by strong acid sites and, in turn, favored by the density of acid sites, is restricted [30]. Moreover, the ability of the mesopores to enhance the mass transfer property, reduces the confinement of coke precursors and the blocking of the micropores of the zeolites that the coke may cause [31].

The desilication of zeolites with NaOH has been widely used to establish a hierarchical porous structure. The most studied one has been the zeolite HZSM-5, since it has been modified for the dehydroaromatization of methane [32], the cracking of *n*-pentane [33] and the conversion of methanol into hydrocarbons [34] and into olefins [35]. Zeolite Y has been also desilicated for being used in catalytic cracking reactions [36], but also for the production of methyl methoxyacetate [37] and for the conversion of coal pyrolysis vapors to light aromatics [38]. Finally, the hydrocracking of a mixture of plastics has been also investigated with zeolites subjected to desilication [39,40].

In the present work, the modification of a commercial HY ultrastable zeolite by means of desilication has been studied with aim of minimizing the overcracking reactions and the deactivation by coke of a PtPd/HY catalyst used in the hydrocracking of HDPE blended with VGO. The desilication has been performed using NaOH as the leaching agent. A detailed analysis of the naphtha and LCO fractions obtained has been carried out, pushing the knowledge beyond the yields and the conversion achieved. Additionally, the nature and location of the carbonaceous residue deposited on the catalysts has been analyzed, comparing the results obtained by desilicated catalyst with those obtained for the parent one. The results of co-feeding the plastic with a real refinery stream expose the interest of the possible scaling up of the proposed managing alternative (Waste Refinery).

2. Experimental

2.1. Feeds

The VGO (Petronor Refinery, Muskiz, Spain) is mainly composed of the gas oil produced in the vacuum distillation column and, in a lesser extent, of the gas oil obtained in the visbreaker and coker units. A subsequent hydrotreatment in a hydrodesulphurization unit has significantly decreased the contents of S and N. Thus, the VGO used has a composition suitable for hydrocracking with noble metals catalysts. Its main physicochemical properties have been summarized in Table S1 and the techniques used for their determination are described in detail elsewhere [24]. In short, the VGO is mainly aromatic, with remarkable contents of di- and poly-aromatics (12.41 and 15.75 wt%, respectively) and naphthenic compounds (35.27 wt%). The simulated distillation analysis yielded contents of 4.5 wt% of light cycle oil (LCO) (216–350 °C) and 95.4 wt% of heavy cycle oil (HCO) (>350 °C).

The high-density polyethylene (HDPE) has been purchased from Dow Chemical (Tarragona, Spain) in the form of 4 mm pellets. Its main properties, i.e. average molecular weight, dispersity, density and higher heating value, have been displayed in Table S1. It is worth mentioning that before being blended with the VGO, the HDPE has been grinded under cryogenic conditions (size < 0.5 mm).

2.2. Catalysts preparation and characterization

Three PtPd catalysts supported on Y zeolite have been used. The zeolite (ultrastable CBV712) has been supplied by Zeolyst International in the ammonium form with a SiO_2/Al_2O_3 ratio of 12. The first catalyst (Cat-A) has been prepared using the zeolite without being submitted to any desilication treatment. The second one (Cat-B), has been prepared after submitting the zeolite to a desilication treatment (detailed below), whereas the third one (Cat-C) has been prepared after submitting twice the zeolite to the desilication treatment.

The alkaline treatment method followed for zeolite desilication has consisted on [31]: i) suspension of 10 g in 300 mL of 0.1 M aqueous NaOH solution and stirring for 15 min at room temperature; ii) neutralization of the suspension with an equivalent amount of 1.0 M HCl solution to quench the desilication treatment. No longer contact times are required since using an aqueous NaOH solution, most of the mesoporosity is developed in the first 15 min [41,42]; iii) the desilicated zeolite was filtered and washed with deionized water; iv) the zeolite was subjected to two subsequent ion exchange cycles of 24 h with a 0.50 M aqueous solution of NH_4Cl at room temperature (zeolite/solution ratio of 1 g/5 mL), in order to ensure that the Na introduced during the leaching stage is totally removed. Lastly, v) the zeolite was filtered, washed with deionized water, dried in an oven at 110 °C for 16 h, and calcined in a muffle at 550 °C, using a heating ramp of 12 °C min^{-1}, and maintaining that temperature for 4 h. In all the cases, the incorporation of the metals (1 wt% of Pt and 0.5 wt% of Pd) has been carried out following the procedure described by Gutiérrez et al. [43]. The behavior of PtPd as a metal function to activate hydrogenation reactions is well established [44]. This bimetallic function offers advantages over each of the individual metals in terms of stability and higher conversion, due to its lower S retention. Moreover, the PtPd catalyst supported on HY zeolite is very stable and has an outstanding capacity for obtaining naphtha and medium distillates [43–45].

The catalysts have been extensively characterized in order to correlate their physicochemical properties with their catalytic behavior. In this way, the textural properties have been determined from the N$_2$ adsorption–desorption isotherms. The crystalline structure of the supports has been analyzed by X-ray diffraction. The acidic properties have been measured by temperature-programmed desorption/cracking of *tert*-butylamine and by pyridine FTIR analysis. The composition of the catalysts and the metal content have been measured by wavelength dispersion X-ray fluorescence spectrometry and inductively coupled

plasma with atomic emission spectroscopy, respectively. In addition, some TEM images have been acquired for characterizing in a higher extent the structure of the catalyst and for observing the metal dispersion. Finally, the coke deposited on the catalysts has been measured by temperature-programmed oxidation. The equipment used for each analysis, as well as the procedures followed are available in the Supplementary Material.

2.3. Experimental set-up and conditions

The experimental set-up used for the hydrocracking tests has been a 100 mL semi-batch stirred tank reactor (Parker Autoclave Engineers) (Fig. S1). A detailed explanation about the setup and the reaction procedure is available in our previous works [24,25]. The reactor has been charged with 40 g of feed, (HDPE, 20 wt%; VGO, 80 wt%), and the corresponding mass of catalyst. Catalyst to feed mass ratio (C/F) has been established at 0.1 g_{cat} g_{charge}^{-1}, which has ensured total plastic conversion [24]. Reactions have been carried out at 80 bar of H_2 pressure, and at 440 °C. Under these conditions, the HDPE is completely dissolved in the VGO. Vigorous and homogenous stinging (1300 rpm) has been used to keep reactant particles in motion, which, together with the high flow rate of gas (100 mL min^{-1}) ensure the absence of external mass transfer limitations [46]. After 120 min of reaction, the reactor was cooled down following a cooling rate of 20 °C min^{-1} using an open water system. The gases have been collected in a sampling bag and analyzed by GC, whereas liquid products have been separated following the solvent fractionation method previously described [24] (Fig. S2). These liquid products have been analyzed as indicated in the following section (Section 2.4).

2.4. Analysis of the products

Reaction products have been fractioned according to their boiling point range into: (i) gas (<35 °C); (ii) naphtha (35–216 °C); (iii) light cycle oil (LCO, 216–350 °C); (iv) heavy cycle oil (HCO, > 350 °C); (v) wax (which can be defined as unconverted HDPE); and (vi) coke (carbonaceous deposit on the catalyst). One should note that both LCO and HCO fractions were already present in the feedstock (Table S1).

The gas products have been analyzed by gas chromatography in an Agilent Technologies 6890 GC gas chromatograph. Liquid products have been submitted to different analysis. Firstly, fraction distribution has been determined by simulated distillation analysis according to ASTM D2887. Secondly, bi-dimensional gas chromatography (Agilent 7890A Series GC Systems coupled to an Agilent 5975C Series GC/MSD mass spectrometer) has been used for analyzing the composition of the naphtha and LCO fractions. It has been grouped in: (i) n-paraffins (n-P); (ii) isoparaffins (i-P); (iii) naphthenes (N); (iv) 1-ring aromatics (A$_1$); (v) 2-ring aromatics (A$_2$), and; (vi) 3$^+$-ring aromatics (A$_{3+}$). Note that the configuration of all the analysis equipment used can be found elsewhere [47].

2.5. Reaction indices

The extent of the hydrocracking reactions has been assessed by considering on one hand, the conversion of the compounds within the HCO fraction into lighter ones and condensed to coke, and; on the other hand, the hydrocracking of the HDPE into liquid hydrocarbons. Thus, the following conversion indices have been defined:

HCO conversion

$$X_{HCO} = \frac{(m_{HCO})_{initial} - (m_{HCO})_{final}}{(m_{HCO})_{initial}} \cdot 100 \tag{1}$$

HDPE conversion

$$X_{HDPE} = \frac{(m_{HDPE})_{initial} - (m_{HDPE})_{final}}{(m_{HDPE})_{initial}} \cdot 100 \tag{2}$$

where $(m_{HCO})_{initial}$ and $(m_{HCO})_{final}$ are the initial and final masses of the HCO fraction, respectively. On the other hand, $(m_{HDPE})_{initial}$ and $(m_{HDPE})_{final}$ are the amount of HDPE fed and the wax obtained as by-product, respectively.

The yield of each fraction (Y_i) has been defined as the mass of fraction i (m_i) formed in relation to initial mass of reactants:

$$Y_i = \frac{m_i}{(m_{VGO} + m_{HDPE})_{initial}} \cdot 100 \tag{3}$$

The selectivity to fuel (S_F) has been determined from the dimensionless catalytic performance parameter proposed by Al-Attas et al. [48]:

$$S_F = \frac{Y_{Naphtha} + Y_{LCO}}{Y_{Gas} + Y_{HCO} + Y_{Wax} + Y_{Coke}} \tag{4}$$

3. Results and discussion

3.1. Catalyst properties

Table 1 shows the main physical properties of the support zeolite and the three catalysts. Small differences can be observed between support zeolite and Cat-A, which exposes that metal deposition has barely affected the zeolite properties. Some differences between N2 adsorption-desorption isotherms isotherms as a result of the desilication treatment can be found in Fig. S3. It can be seen a reduction of the adsorbed volume at low relative pressures, which is correlated with a reduction of the microporous surface [49]. Therefore, the micropore area is strongly affected by the zeolite crystal destruction caused by the desilication treatment. In this way, the micropore area follows the trend: Cat-A > Cat-B > Cat-C. The same conclusion can be obtained for the surface area (S_{BET}) when alkaline treatment is applied. Thus, Cat-A is mainly microporous (543 of 620 m^2/g) but the catalysts that have been submitted to basic leaching with the NaOH solution show less microporous area, especially Cat-C (377 of 478 m^2/g). Consequently, the micropore volume of Cat-B and Cat-C has been also reduced reaching values of 0.20 and 0.17 cm^3 g^{-1}, respectively, that are below of 0.24 cm^3 g^{-1} of Cat-A. The volume of the mesopore follows an opposite trend, increasing with the severity of desilication from 0.17 cm^3 g^{-1} for Cat-A to 0.20 cm^3 g^{-1} for Cat-B and to 0.25 cm^3 g^{-1} for Cat-C. Furthermore, since the average pore diameter (d$_p$) is strongly related to the mesopore area, an increase of the latter entails an increase of the former. Therefore, the average mesopore diameter has increased from 8.4 nm (Cat-A) to 10.2 nm (Cat-C). These changes in physical properties with desilication treatment, with an increase in mesopore volume and a decrease in micropore volume, are in line with those previously reported by other authors for different zeolites [31,36,50].

Analyzing the XRD patterns (Fig. 1) it can be observed that the alkaline attack reduces the crystallinity of the zeolite, as reflected by the decrease in the intensity of peaks, at the same time that increases the amorphousness, which is reflected in the background elevation between 20 and 30°. The loss of the crystallinity is associated with the selective removal of Si from the zeolite framework [36]. However, as it will be discussed latter (Table 2), the bulk content of Si remains essentially constant, suggesting that the Si species would end up as an amorphous extraframework phase. This behavior in XRD patterns has been also

Table 1
Textural properties of the catalysts.

	Zeolite	Cat-A	Cat-B	Cat-C
S$_{BET}$ (m^2 g^{-1})	799	620	535	478
S$_{micro}$ (m^2 g^{-1})	685	543	448	377
S$_{meso}$ (m^2 g^{-1})	114	77	87	101
V$_{micro}$(cm^3 g^{-1})	0.27	0.24	0.20	0.17
V$_{meso}$(cm^3 g^{-1})	0.17	0.17	0.20	0.25
d$_p$ (nm)	8.7	8.4	9.6	10.2
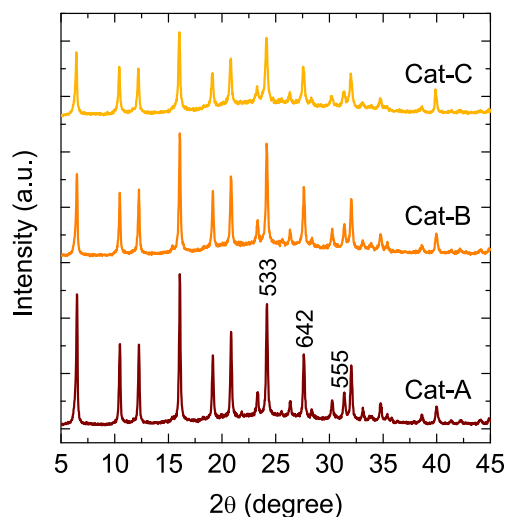
Fig. 1. XRD patterns of the catalysts.

Table 2
Chemical composition of the catalysts.

	Cat-A	Cat-B	Cat-C
SiO_2 (wt%) [a]	87.15	87.35	86.91
Al_2O_3 (wt%) [a]	12.06	11.13	10.90
Si/Al [b]	11.44	10.83	10.24
Pt (wt%) [c]	1.19	1.13	1.11
Pd(wt%) [c]	0.53	0.49	0.47

Measured by means of: [a] WDXRF; [b] XRD; [c] ICP-AES.

observed by Gackowski et al. [36].

Thus, the desilication treatment barely changes the total content of Si as it has been obtained in the WDXRF analyses (Table 2). However, the content of Al_2O_3 slightly decreased when the number of desilication cycles increased. Nevertheless, as mentioned by Qin et al. [51], XRF does not only measure the amount of SiO_2 and Al_2O_3 in the zeolite framework, but also in the amorphous phase. Therefore to identify the Si and Al that correspond to the crystalline phase an additional technique would be required, such as X-ray diffraction (XRD) [36,51] or nuclear magnetic resonance (NMR) [52].

Consequently, the XRD results depicted in Fig. 1 have been used for determining the Si/Al ratio of the zeolite, which are shown in Table 2. For this purpose, the Breck-Flanigen correlation has been used. The procedure has been explained in detail in the Supplementary Material. According to these results, it can be seen that the Si/Al ratio decreases from 11.44 in Cat-A to 10.83 and 8.01 in Cat-B and Cat-C, respectively. These results expose the effective Si removal from the zeolite crystals.

Regarding the metal content of the catalysts (Table 2), it can be seen that the values obtained by means of ICP-AES analysis are close to the nominal ones (1 and 0.5 wt%, respectively), which reveals that metal incorporation has been carried out successfully. However, attending to the values it can be seen that the lower the crystallinity of the support, the lower the contents of Pt and Pd.

In Fig. S4 it can be seen the profile of released butane obtained in the TPD of *tert*-butylamine (*t*-BA) for all the catalysts. The quantitative results collected in Table 3 display a reduction in the total acidity after

Table 3
Acidic properties of the catalysts.

	Cat-A	Cat-B	Cat-C
Total Acidity (mmol$_{t-BA}$ g^{-1})	1.7	1.2	0.9
Acid strength (kJ mol$_{t-BA}^{-1}$)	135	147	150
Brønsted/Lewis ratio	1.53	1.93	2.40

successive desilication treatments from 1.7 to 0.9 mmol$_{t-BA}$ g^{-1} in Cat-A and Cat-C, respectively. The same behavior was observed by Gayubo et al. [53] since they obtained a reduction of the total acidity for the desilicated HZSM-5 zeolites. Furthermore, Fig. S4 shows that TPD signals are attenuated from Cat-A to Cat-B and, in a higher extent, to Cat-C. Thus, the two desilication steps the Cat-C has been submitted to, have notably reduced the acidity of the catalyst. Small differences in butane release temperature are observed for Cat-A, Cat-B and Cat–C, with peaks at 238, 236 and 235 °C, respectively. However, the effect of desilication over the acid strength is evident in the value of the heat of adsorption of this base, which increases from 135 kJ mol$_{t-BA}^{-1}$ for Cat-A to 147 and to 150 kJ mol$_{t-BA}^{-1}$ for Cat-B and Cat-C, respectively. It exposes a slight increase of the acid strength of the residuary acid sites after the desilication treatment. These results are in line with those obtained by Li et al. [49], who compared the acidic properties (measured by NH$_3$-TPD) of a parent HZSM-5 zeolite and an alkali treated one.

The spectra obtained in the FTIR of pyridine have been used to identify the nature of the acidic sites (Fig. S5). The results in Table 3 show that the calculated B/L ratio is 1.53 for Cat-A and that the desilication treatment leads to an increase in the B/L ratio for Cat-B (1.93), which would be consistent with the decrease in the Si/Al ratio in Table 2. These results are in line with those reported by Gil et al. [52] in the desilication of a HZSM-5 zeolite, who obtained a higher reduction in Lewis sites. Finally, the double desilication steps to which Cat-C has been submitted lead to a further reduction in the numbers of both Brønsted and Lewis sites. Nonetheless, the latter are further reduced again to a greater extent obtaining the highest B/L ratio, 2.40 (Table 3). Gackowski et al.[36] emphasized the need to limit the severity of NaOH desilication to control the removal of strong acid sites from the HY zeolite, proposing a mixture of NaOH and TBAOH (tetrabutylammonium hydroxide) for desilication. The randomly removal of Si and of Al under severe desilication conditions with NaOH has been reported in the literature [33,54,55]. From the results in Table 3 of the increase of the Brønsted/Lewis acidic sites ratio with desilication it can be deduced that this desilication is moderate, and the zeolite maintains a remarkable level of acid strength, which is required for cracking purposes.

Fig. 2 shows the TEM images of parent (Cat-A) and desilicated (Cat-B and Cat-C) catalysts. Cat-A (Fig. 2a and b) shows a smooth surface with an excellent dispersion of Pt and Pd particles (small dark dots). This moderate dispersion of the metallic crystallites is suitable for their stability, since high dispersion favors sintering. The mesopores emerge with different diameter when desilication is carried out and these can be clearly observed in Fig. 2c that corresponds to Cat-B. It displays a clear degradation of the surface due to the alkali-treatment, exposing that that most of the mesopores formed are presumably located on the outermost surface of the particle [56]. However, the alkaline treatment is not observed to have changed the dispersion of the metallic phase dispersion (Fig. 2d). Fig. 2e shows the superficial state of the catalyst after two desilication cycles (Cat–C). As reported in the literature [32], the more severe the desilication conditions, the more extended the degradation of the catalyst (in terms of modifications of acidity and porosity). In this case, a harder degradation can be observed, which has formed larger mesopores (Fig. 2e), but has not affected the dispersion of the metal particles (Fig. 2f). So, the metal function properties (such as dispersion) are found to be barely affected by alkaline treatment of the zeolite.

3.2. Conversion and yields

The catalysts have been tested under quite harsh operating conditions, especially the temperature of 440 °C, as shown by the formation of gas and condensation to coke. The yields of the different products, as well as the conversion obtained with each catalyst have been collected in Fig. 3. As it can be seen, both textural and acidic properties affect both conversions and product distribution. With Cat-A, which is the most acidic one and has the highest amount of Brønsted acid sites, total HDPE conversion (100 %) and the highest HCO conversion (91.1 %) have been
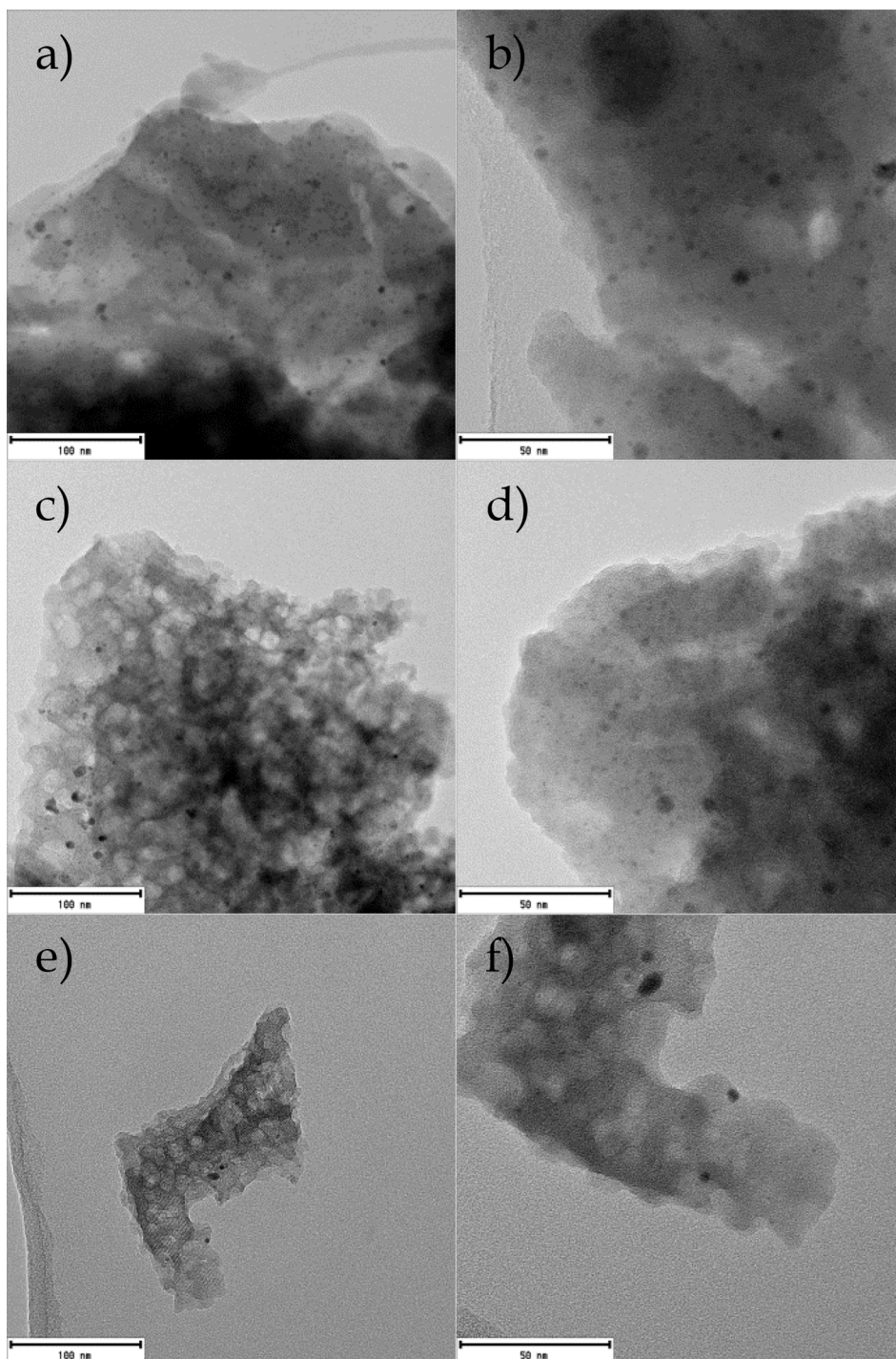
Fig. 2. TEM images obtained for Cat-A (a and b), Cat-B (c and d) and Cat-C (e and f).

achieved, as well as proper naphtha and LCO yields (31.3 and 9.3 wt%, respectively). However, the aforementioned acidic properties, together with the larger micropore volume resulted in an excessive gas formation (49.6 wt%) and a high coke formation (3.1 wt%).

The decrease in total acidity and the amount of Brønsted sites caused by the desilication treatment, resulted in a decrease in the conversion levels obtained with Cat-B. In this way, values of 86 and 81.5 % have been obtained for X_{HDPE} and X_{HCO}, respectively. The changes in the properties of the catalyst have also affected the yield of naphtha and, especially, that of gases. In this way, a reduction of the overcracking reactions has reduced the yield of gases to 28.2 wt%, whereas that of naphtha has increased to 42.9 wt%. This is because the weaker catalyst

properties hinder the hydrocracking mechanism of hydrocarbon compounds of VGO [57,58]. In this mechanism, alkanes in the naphtha fraction dehydrogenate to alkenes at the metal sites, and this is where the hydrogenation/dehydrogenation power of the metallic phase is extremely relevant. Desorption of the formed alkenes from the metal site and subsequent migration to the Brønsted acid sites occurs, where they are protonated to secondary alkylcarbenium ions. It is rare that β-scission of the secondary alkyl carbene ions occurs to form a smaller alkyl carbenium ion and an alkene so that the reaction by-product is energetically disadvantaged, although the rate of this reaction increases as the branching of the secondary alkyl carbene ions increases. Therefore, skeletal rearrangement to monobranched alkylcarbenium ions is more
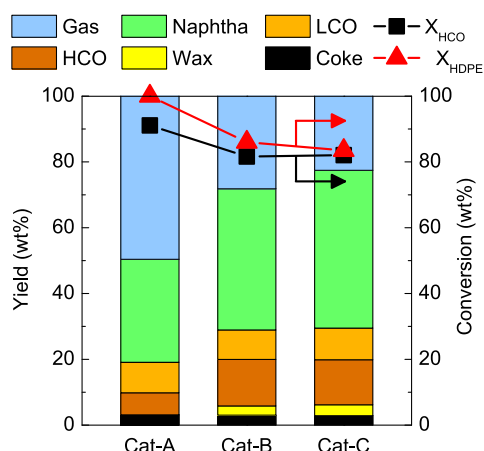
Fig. 3. Yields and conversions for each catalyst.

likely to occur, where they desorb from the acid sites and diffuse to the metal sites, hydrogenating to the corresponding isoparaffins. As the conversion proceeds, the monobranched paraffins are converted to di-branched paraffins and so on.

However, the LCO yield is not affected by desilication, being almost the same as that obtained with Cat-A (8.9 wt%). Similarly, Munir et al. [39] reported that there is no significant change in the yield of LCO using desilicated beta zeolite based catalysts in the hydrocracking of waste plastic. The behavior of LCO fraction owes to two opposite effects that are promoted with desilication. On one hand, the desilication promotes the diffusion of the bulky molecules within the HCO fraction into the newly created mesopores that increases their conversion into LCO molecules. The creation of these mesopores has been quantified in Table 1. In contrast, the lower acidity of the desilicated catalysts discourages the cracking of the LCO molecules into molecules within the naphtha fraction. The lower HCO conversion with Cat-B (Fig. 3) highlights the greater importance of acidity decrease in catalyst performance. The aromatics present in the HCO fraction will also be hydrogenated at the metal sites to their corresponding naphthenes (or polynaphthenes in the case of PAHs). The ring opening of naphthenes to form olefins is thermodynamically favored. These olefins, in turn, will hydrogenate at the metal sites to form paraffins. There is therefore a synergistic effect between the two stages, the first hydrogenation stage and the subsequent cracking stage, with the second stage shifting the thermodynamic equilibrium of the hydrogenation reactions. Thus, considering the feed composition, the co-feeding of HDPE together with VGO will lead to the rapid formation of secondary alkylcarbenium ions by protonation of the free radicals formed from the HPDE chains [59], triggering the mechanism mentioned for the hydrocracking of the VGO components (alkanes and aromatics).

The yield of coke is also slightly reduced because of the widening of the porous structure and a value of 3 wt% has been obtained for Cat-B.

Concerning the results obtained with Cat-C, small differences have been obtained in terms of conversion when comparing with Cat-B. However, Cat-C has offered higher yields of naphtha and LCO at the same time that those of gas and coke have been reduced. These facts lay on the following parameters. Firstly, a slight decrease of the total acidity of Cat-C with respect to that of Cat-B (0.9 and 1.2 $mmol_{t-BA}$ g^{-1}, respectively), which resulted in a decrease of the overcracking activity that tends to convert the molecules within the naphtha fraction into gases. Secondly, the higher mesoporosity in Cat-C (0.25 cm^3 g^{-1}) together with the higher average pore diameter that favour the accessibility of the bulky molecules within the LCO and HCO fractions to the inner acidic sites. This fact counteracts the lower density of acid sites of Cat-C, offering similar conversion levels than Cat-B. Thirdly, the decreased observed in the conversion of plastic exposes that the

attenuation of the acidity has a greater impact than the improved accessibility of the macromolecular chains of the plastic. Fourthly, the decrease in acidity and the increased presence of mesopores and the reduction of the micropores contribute to attenuate the coke deposition, which decreases down to 2.9 wt% for Cat-C. Similar results were observed in different reactions by other authors who increased the severity of the zeolite desilication treatment, thus reducing the yield of coke [50,60–62].

To assess the effect of zeolite desilication on the catalyst ability to generate liquid fuels in the hydrocracking process, in Fig. 4 has been depicted the selectivity to fuel parameter. It can be seen that the alkaline leaching has a positive effect on this parameter, which is 0.7 for Cat-A and increases up to 1.1 and 1.4 for Cat-B and Cat-C, respectively. Thus, the formation of naphtha has been maximized, since that of LCO remains steady.

3.3. Composition of the gas fraction

The composition of the gas fraction obtained with each of the catalysts has been depicted in Fig. 5, which can be used for assessing the effect of the desilication of the zeolite. As it was expectable, the gas fraction is just composed by paraffins. On one hand, CH_4 and C_2H_6 that are known as dry gas, and the other hand, C_3H_8, $i-C_4H_{10}$ and $n-C_4H_{10}$, which are commonly grouped into liquefied petroleum gases (LPG). Attending to the composition obtained with Cat-A, the main components are C_3 and C_4 compounds with concentrations of 46.5 and 17.2 wt%, respectively, whereas the dry gas accounts for 36.6 wt% being ethane the main compound (25.5 wt%).

For Cat-B, the concentration of CH_4 and C_2H_6 increases to 19.1 and 28.2 wt%, respectively. The higher concentration of dry gas in gas products, in relation to LPG, with the modified catalysts, is explained by the fact that the attenuation of total acidity caused by the desilication process has reduced the overcracking activity of the catalyst that converts naphtha molecules into LPG. However, that attenuation exposes in a higher extent the remaining thermal cracking activity, which tends to produce low molecular weight gas products (C_1 and C_2) by means of free radical mechanisms. This trend of increasing relative relevance of thermal cracking when the extent of catalytic cracking diminishes is described in the literature [63–65]. At the same time, the desilication reduced the yield of the LPG fraction. Attending to its composition, the proportions of C_3H_8 and $n–C_4H_{10}$ in LPG have been reduced whereas that of $i-C_4H_{10}$ has increased (34.7, 6.6 and 11.2 wt%, respectively). However, it is important to notice that the yield of $i-C_4H_{10}$, observed with desilicated catalysts (3.2 wt% with Cat-B and 2.7 wt% with Cat-C), were noticeably lower than that observed with the parent catalyst (4.95
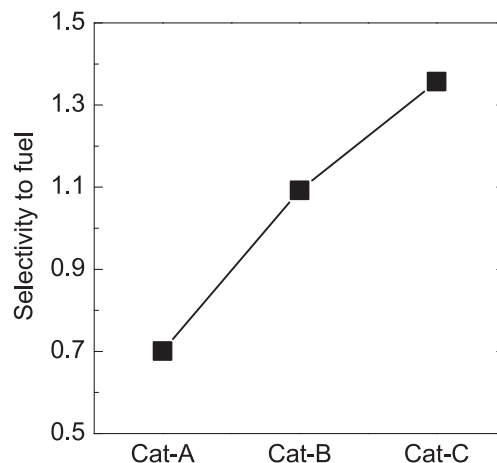

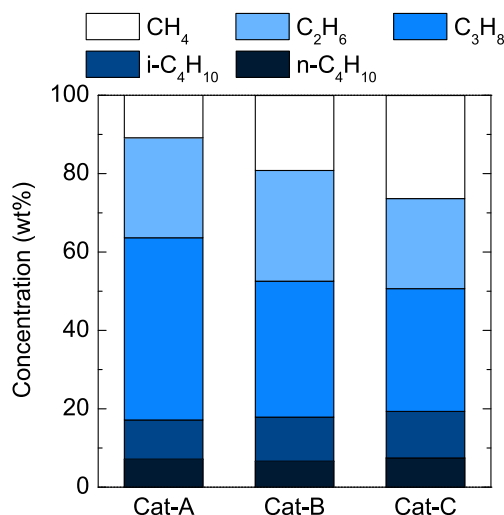**Fig. 4.** Values obtained with the three catalysts for the selectivity to fuel parameter.

Fig. 5. Effect of zeolite desilication on gas composition.

wt% with Cat-A). This is an expected behavior, given that the yield of i-C_4H_{10} is a good indicator of catalytic cracking [66]. Consequently, the decrease in total acidity in the desilicated zeolites reduced their cracking activity as compared with unmodified catalyst.

Finally, the composition of the gas fraction obtained with Cat-C is quite similar to that obtained with Cat-B, given that both catalysts have a significantly lower acidity than Cat-A. Continuing with previously observed trend, the LPG concentration slightly diminishes with Cat-C, representing almost half of the gas. Within LPG fraction, C_4 grows stepwise (both i-C_4H_{10} and n-C_4H_{10} are slightly higher than those obtained with Cat–B) meanwhile C_3H_8 decreases, being these concentrations 19.3 and 31.3 wt%, respectively.

3.4. Composition of the naphtha fraction

Apart from attenuating the overcracking of the naphtha fraction, desilication treatment has a noticeable effect on its composition as shown in Fig. 6. It is remarkable the progressive reduction of the content of aromatics with the desilication cycles. In this way, the naphtha fraction obtained with Cat-A has the highest total content of aromatics (55.5 wt%) that has been reduced down to 33.3 wt% for Cat-C. The concentration of naphthenes has followed the same trend as that of aromatics and it has passed from 16.6 wt% for Cat-A to 8 wt% for Cat-C. Consequently, the concentration of saturated compounds, i.e. normal and ramified paraffins, has increased to reach a maximum concentration
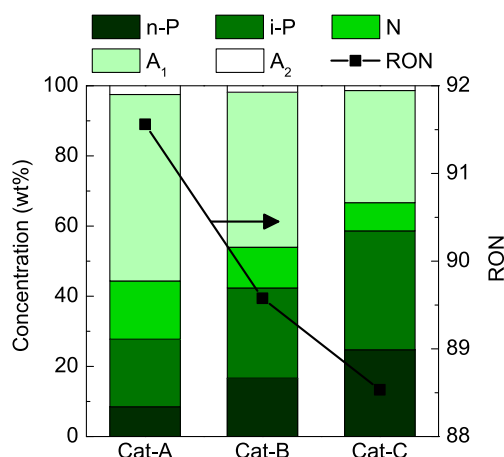
of 58.5 wt% for Cat-C. Garcia et al. [31] reported similar trends for the concentration of the aliphatic and aromatic compounds in the naphtha fraction obtained in the catalytic cracking of bio-oil using desilicated zeolite-based catalysts.

Considering that desilication decreases the level of HCO conversion reached and that the yield of LCO remains practically constant (Fig. 3), it can be assumed that both the acidity attenuation (Table 3) and the presence of mesopores (Table 1) in the desilicated catalysts have contributed to modify the composition of the naphtha fraction. Indeed, these properties have affected the overcracking reactions and the interconversion reactions within the naphtha fraction. The results can be explained through the decreased acidity in the desilicated samples that attenuates both the cracking activity that converts the paraffins into lighter gas products and the cyclization reactions that end with the formation of aromatics. In addition, the lower acidity of the catalyst will presumably lead to an attenuation of the conversion of mono- and di-aromatics from the LCO.

In order to fully characterize the naphtha fraction obtained, the research octane number (RON) of this fraction has been also determined according to the procedure explained by Anderson et al. [67]. In this way, it can be seen that the RON follows a decreasing trend with the increase in the desilication degree. This decrease is a direct consequence of the reduction of the concentration of aromatics in the naphtha fraction. Anyway, the values of the RON obtained with all the catalysts were quite high, since with Cat-A a value of 91.6 has been obtained that was subsequently reduced to 89.6 and 88.5 with Cat-B and Cat-C, respectively.

3.5. Composition of the LCO fraction

Fig. 7 shows the composition of the LCO fraction obtained with the three catalysts. The desilication of the zeolite has resulted in an increasing concentration of aromatics in the LCO fraction. It has gone from 32.9 wt% for Cat-A to 56.9 wt% for Cat-C. This higher aromatic concentration after desilication was also observed by Tarach et al. [56] in the hydrocracking of VGO. The concentration of paraffins (n-P and i-P), in turn, has decreased going from 67.1 wt% for Cat-A to 41.5 wt% for Cat-C. Finally, the concentration of naphthenes in the LCO fraction is trivial. However, it has increased from 0.1 wt% for Cat-A to 1.6 wt% for Cat-C.

The increase in the concentration of aromatics can be mainly attributed to the lower total acidity of desilicated catalysts that are incapable of converting the aromatics into lighter ones within the naphtha fraction. So, presumably, the effect of the decrease in acidity is more important than the presence and increase of mesopores (Table 1).
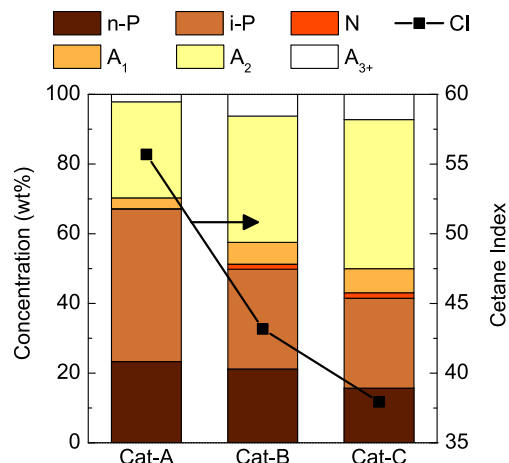

Fig. 6. Effect of zeolite desilication on the composition of the naphtha fraction and RON obtained for the three catalysts.

Fig. 7. Effect of zeolite desilication on the composition of the LCO fraction and CI obtained for the three catalysts.

Thus, although the access to the acid sites of the catalyst of the poly-aromatics in the HCO will be favored, the capacity of the catalyst for further cracking them has been reduced. That is, the acidity of Cat-B and, especially, Cat-C is insufficient for the cracking of the intermediates derived from the partial hydrogenation of the aromatic compounds, which is a key step in order to shift the system to a more favorable condition, given that these reactions are limited by the thermodynamic equilibrium [64]. In addition, high temperatures (such as 440 °C) and the reduction of acidic sites promote the dehydrogenation reactions that form aromatics on the metal sites of the catalyst, as well as the condensation reactions of light aromatics within the naphtha fraction to heavier aromatics within the LCO fraction. Therefore, these results reinforce the arguments aforementioned about the reduction of aromatics in the naphtha fraction using desilicated catalysts. The composition of the naphtha and LCO fractions are closely interrelated to the fact that aromatics in the naphtha fraction are coming from the LCO fraction, according to the hydrodearomatization mechanism established by Karakhanov et al. [65].

To fully characterize the LCO fraction obtained, the cetane index (CI) of this fraction has been calculated according to a modified ASTM D4737 Standard. It must be considered that the CI is inversely correlated with the concentrations of aromatic compounds and branched hydrocarbons [44]. The values of CI obtained (55.7, 43.1 and 37.9, for Cat-A, Cat-B and Cat-C, respectively) are higher than those previously reported by Gutierrez et al. [45] in the hydrocracking of LCO (ca. 30), but lower (ca. 70) than those obtained by Escola et al. [68] in the hydrocracking of neat plastic.

3.6. Coke deposition

The effect of zeolite desilication on coke deposition has been studied by temperature-programmed oxidation (TPO) analysis, the methodology of which has been described in the Supplementary Material. This technique provides information on the quantity, nature and location of the coke [69]. The TPO profiles for the three catalysts are plotted in Fig. 8. Clearly, these profiles can be deconvoluted into two peaks. It is well established in the literature [69–71] that the first peak, at a range of low temperatures (375–475 °C) can be associated with a fraction of the coke deposited on the external surface of the zeolite crystals (which will be named coke I) and the combustion of which is not limited by diffusional limitations. This coke usually has a poorly developed structure, with a moderate H/C ratio. In contrast, the second peak obtained at

higher temperature (475–550 °C) corresponds to the fraction of coke located inside the crystalline channels of the zeolite (named coke II), whose combustion is hindered by diffusional limitations. This diffusional restrictions increase the residence time of the molecules within the inner channels of the zeolite increasing their tendency to condensate ending in polyaromatic structures [71]. Consequently, even though under high H_2 pressure the reactions leading to polyaromatic structures are more inhibited than in the absence of H_2 as it has been checked by Palos et al. [72], coke II is more developed (lower H/C ratio) than coke I.

Table 4 displays the results obtained in the deconvolution of the TPO profiles plotted in Fig. 8. The total amount of coke obtained for Cat-A is 28.7 wt% and the amount of both types of coke is similar (proportions close to 50 wt%). However, desilication has caused a decrease of the total content of coke to 27.2 and 24.7 wt% for Cat-B and Cat-C, respectively. Furthermore, the fraction of coke I has increased for Cat-B up to 74.8 wt% and, even higher, for Cat-C reaching a value of 77.4 wt%. The differences that desilication has brought can be related to the changes caused in the in the properties of the catalysts that have modified the concentration of the possible precursors of both types of coke. Thus, the lower total acidity and lower density of strong acidic sites of desilicated catalysts attenuate the extent of the condensation reactions of the aromatic coke precursors inside the crystalline channels of the zeolite, decreasing the formation of coke II.

In addition, the higher free volume in the porous structure formed by the desilication treatment, with a higher presence of mesopores (Table 1), facilitates the circulation of coke precursors out of the channels of the zeolite leading to the formation of coke I. Indeed, the reduction of the temperature of the maximum burning rate of coke I observed for Cat-B and Cat-C with respect to that of Cat-A (Fig. 8) indicates that the diffusional restrictions during the combustion process have been reduced and that coke I in desilicated catalysts is formed by less developed structures. The higher absolute content of more condensed coke (coke II, Table 4) obtained with the parent catalyst (Cat-A) is in concordance with the higher conversions of HDPE and HCO, as compared with those observed with modified catalysts (Cat-B and Cat-C, Fig. 3). The temperature that corresponds to the maximum combustion rate of coke II is the same for all the catalysts (500 °C). This fact lays on the location of the coke in the channels of the zeolite and the combustion of which will be conditioned by the diffusion limitations of the air.

4. Conclusions

Zeolite desilication is an effective treatment to improve the performance of the PtPd/HY catalyst for the hydrocracking of a mixture of HDPE (20 wt%) and VGO, since it decreases the total acidity at the same time that promotes the creation of mesopores in the zeolite. These modifications result in a significant increase of the yield of naphtha, due to the attenuation of the overcracking of this fraction to gas products. For example, the yield of naphtha observed with unmodified catalyst (31.3 wt%, Cat-A) was increased to 42.9 wt% and 48.0 wt% with Cat-B and Cat-C, respectively. In addition, the naphtha fraction obtained has a lower content of aromatics and a higher content of paraffins, which will facilitate its subsequent reforming in the refinery for its incorporation into the pool of commercial gasoline. It is also noteworthy that less coke is deposited on the modified catalysts, and that in the catalysts subjected to desilication this deposition occurs preferentially on the outside of the crystalline channels of the zeolite.

The desilication of the zeolite has as a counterpoint a slightly lower
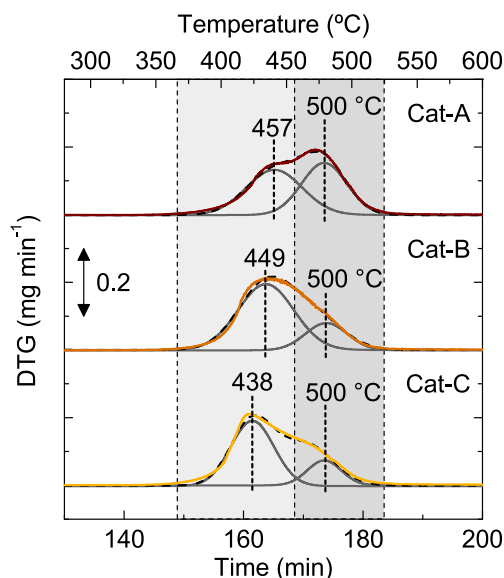
Fig. 8. TPO profiles of the coke combustion deposited on the three catalysts.

Table 4
Deconvolution results of TPO profiles.

	Cat-A	Cat-B	Cat-C
Coke content (wt%)	28.7	27.2	24.7
Fraction of Coke I (wt%)	48.3	74.8	77.4
Fraction of Coke II (wt%)	51.7	25.2	22.6

conversion of HDPE (which remains above 80 wt%) and of the heavy components (fraction of HCO) in the VGO fed. The LCO fraction yield is barely affected, although the concentration of aromatics is higher and the concentration of paraffins is lower than with the parent catalyst (Cat-A).

These results are of interest for progressing towards the large-scale valorization of polyolefins (just as the HDPE) by co-feeding them with VGO. In this way, two goals could be achieved concurrently: (i) the rational management of waste plastics, and (ii) the intensification of oil valorization.

CRediT authorship contribution statement

Francisco J. Vela: Investigation, Formal analysis, Writing – original draft. **Roberto Palos:** Writing – original draft, Writing – review & editing, Visualization, Conceptualization. **Juan Rafael García:** Investigation, Formal analysis, Writing – review & editing. **Ulises Sedran:** Writing – review & editing, Conceptualization. **Javier Bilbao:** Writing – review & editing, Supervision, Project administration, Funding acquisition. **José M. Arandes:** Resources, Project administration, Funding acquisition. **Alazne Gutiérrez:** Writing – original draft, Supervision, Methodology, Visualization, Conceptualization.

Declaration of Competing Interest

The authors declare that they have no known competing financial interests or personal relationships that could have appeared to influence the work reported in this paper.

Acknowledgements

Appendix A. Supplementary data

Supplementary data to this article can be found online at https://doi.org/10.1016/j.fuel.2022.125392.

References

[1] De Fano D, Schena R, Russo A. Empowering plastic recycling: empirical investigation on the influence of social media on consumer behavior. Resour Conserv Recycl 2022;182:106269. https://doi.org/10.1016/j.resconrec.2022.106269.

[2] Geyer R, Jambeck JR, Law KL. Production, use, and fate of all plastics ever made. Sci Adv 2017;3:e1700782.

[3] Delaeter C, Spilmont N, Bouchet VMP, Seuront L. Plastic leachates: bridging the gap between a conspicuous pollution and its pernicious effects on marine life. Sci Total Environ 2022;826:154091. https://doi.org/10.1016/j.scitotenv.2022.154091.

[4] Yuan Z, Nag R, Cummins E. Ranking of potential hazards from microplastics polymers in the marine environment. J Hazard Mater 2022;429:128399. https://doi.org/10.1016/j.jhazmat.2022.128399.

[5] Sajjad M, Huang Q, Khan S, Khan MA, Liu Y, Wang J, et al. Microplastics in the soil environment: a critical review. Environ Technol Innov 2022;27:102408.

[6] Hu K, Yang Y, Zuo J, Tian W, Wang Y, Duan X, et al. Emerging microplastics in the environment: properties, distributions, and impacts. Chemosphere 2022;297:134118.

[7] Patrício Silva AL, Prata JC, Walker TR, Duarte AC, Ouyang W, Barceló D, et al. Increased plastic pollution due to COVID-19 pandemic: Challenges and recommendations. Chem Eng J 2021;405:126683.

[8] Lopez G, Artetxe M, Amutio M, Alvarez J, Bilbao J, Olazar M. Recent advances in the gasification of waste plastics. A critical overview. Renew Sustain Energy Rev 2018;82:576–96. https://doi.org/10.1016/J.RSER.2017.09.032.

[9] Lopez G, Artetxe M, Amutio M, Bilbao J, Olazar M. Thermochemical routes for the valorization of waste polyolefinic plastics to produce fuels and chemicals. A review. Renew Sustain Energy Rev 2017;73:346–68.

[10] Soni VK, Singh G, Vijayan BK, Chopra A, Kapur GS, Ramakumar SSV. Thermochemical recycling of waste plastics by pyrolysis: a review. Energy Fuels 2021;35:12763–808. https://doi.org/10.1021/acs.energyfuels.1c01292.

[11] Qureshi MS, Oasmaa A, Pihkola H, Deviatkin I, Tenhunen A, Mannila J, et al. Pyrolysis of plastic waste: opportunities and challenges. J Anal Appl Pyrolysis 2020;152:104804.

[12] Palos R, Gutiérrez A, Vela FJ, Olazar M, Arandes JM, Bilbao J. Waste refinery: the valorization of waste plastics and end-of-life tires in refinery units. A review. Energy Fuels 2021;35:3529–57. https://doi.org/10.1021/acs.energyfuels.0c03918.

[13] Palos R, Gutiérrez A, Arandes JM, Bilbao J. Catalyst used in fluid catalytic cracking (FCC) unit as a support of NiMoP catalyst for light cycle oil hydroprocessing. Fuel 2018;216:142–52. https://doi.org/10.1016/j.fuel.2017.11.148.

[14] Palos R, Gutiérrez A, Fernández ML, Trueba D, Bilbao J, Arandes JM. Upgrading of heavy coker naphtha by means of catalytic cracking in refinery FCC unit. Fuel Process Technol 2020;205:106454. https://doi.org/10.1016/j.fuproc.2020.106454.

[15] Ibarra Á, Hita I, Arandes JM, Bilbao J. Influence of the composition of raw bio-oils on their valorization in fluid catalytic cracking conditions. Energy Fuels 2019;33:7458–65. https://doi.org/10.1021/acs.energyfuels.9b01527.

[16] Bouzouita D, Lelevic A, Lorentz C, Venderbosch R, Pedersen TH, Geantet C, et al. Co-processing bio-liquids with vacuum gasoil through hydrocracking. Appl Catal B Environ 2022;304:120911.

[17] Valle B, Palos R, Bilbao J, Gayubo AG. Role of zeolite properties in bio-oil deoxygenation and hydrocarbons production by catalytic cracking. Fuel Process Technol 2022;227:107130. https://doi.org/10.1016/j.fuproc.2021.107130.

[18] Wang H, Dai F, Yang Y, Li Z, Li C, Zhang S. Catalyst grading optimization and kinetic simulation of the shale oil hydrotreating process. Energy Fuels 2017;31:4353–60. https://doi.org/10.1021/acs.energyfuels.6b02720.

[19] Saab R, Polychronopoulou K, Zheng L, Kumar S, Schiffer A. Synthesis and performance evaluation of hydrocracking catalysts: a review. J Ind Eng Chem 2020;89:83–103. https://doi.org/10.1016/j.jiec.2020.06.022.

[20] Kim CH, Hur YG, Lee K-Y. Relationship between surface characteristics and catalytic properties of unsupported nickel-tungsten carbide catalysts for the hydrocracking of vacuum residue. Fuel 2022;309:122103. https://doi.org/10.1016/j.fuel.2021.122103.

[21] Browning B, Alvarez P, Jansen T, Lacroix M, Geantet C, Tayakout-Fayolle M. A Review of thermal cracking, hydrocracking, and slurry phase hydroconversion kinetic parameters in lumped models for upgrading heavy oils. Energy Fuels 2021;35:15360–80. https://doi.org/10.1021/acs.energyfuels.1c02214.

[22] Vivas-Báez JC, Pirngruber GD, Servia A, Dubreuil A-C, Pérez-Martínez DJ. Impact of feedstock properties on the deactivation of a vacuum gas oil hydrocracking catalyst. Energy Fuels 2021;35:12297–309. https://doi.org/10.1021/acs.energyfuels.1c00965.

[23] Palos R, Gutiérrez A, Arandes JM, Bilbao J. Upgrading of high-density polyethylene and light cycle oil mixtures to fuels via hydroprocessing. Catal Today 2018;305:212–9. https://doi.org/10.1016/j.cattod.2017.06.033.

[24] Vela FJ, Palos R, Bilbao J, Arandes JM, Gutiérrez A. Effect of co-feeding HDPE on the product distribution in the hydrocracking of VGO. Catal Today 2020;353:197–203. https://doi.org/10.1016/j.cattod.2019.07.010.

[25] Vela FJ, Palos R, Trueba D, Bilbao J, Arandes JM, Gutiérrez A. Different approaches to convert waste polyolefins into automotive fuels via hydrocracking with a NiW/HY catalyst. Fuel Process Technol 2021;220:106891. https://doi.org/10.1016/J.FUPROC.2021.106891.

[26] Dik PP, Danilova IG, Golubev IS, Kazakov MO, Nadeina KA, Budukva SV, et al. Hydrocracking of vacuum gas oil over NiMo/zeolite-Al2O3: influence of zeolite properties. Fuel 2019;237:178–90.

[27] Li T, Tao Z, Hu C, Zhao C, Yi F, Zhao G, et al. Brønsted acidity of amorphous silica-aluminas for hydrocracking of Fischer-Tropsch wax into diesel fractions. Appl Catal A Gen 2022;630:118439.

[28] Jia X, Khan W, Wu Z, Choi J, Yip ACK. Modern synthesis strategies for hierarchical zeolites: bottom-up versus top-down strategies. Adv Powder Technol 2019;30:467–84. https://doi.org/10.1016/j.apt.2018.12.014.

[29] Mesa H, Faro Jr A, Rodrigues V. Optimization and study of the response surface of properties for the synthesis of ZSM-5 zeolites with hierarchical pore structure obtained by desilication. J Braz Chem Soc 2021;32:1193–202. https://doi.org/10.21577/0103-5053.20210020.

[30] Kim Y-S, Cho K-S, Lee Y-K. Structure and activity of Ni2P/desilicated zeolite β catalysts for hydrocracking of pyrolysis fuel oil into benzene, toluene, and xylene. Catalysts 2020;10:47. https://doi.org/10.3390/catal10010047.

[31] García JR, Bertero M, Falco M, Sedran U. Catalytic cracking of bio-oils improved by the formation of mesopores by means of y zeolite desilication. Appl Catal A Gen 2015;503:1–8. https://doi.org/10.1016/j.apcata.2014.11.005.

[32] Su L, Liu L, Zhuang J, Wang H, Li Y, Shen W, et al. Creating mesopores in ZSM-5 zeolite by alkali treatment: a new way to enhance the catalytic performance of methane dehydroaromatization on Mo/HZSM-5 catalysts. Catal Lett 2003;91(3/4): 155–67.

[33] Wang Z, Zhang R, Wang J, Yu Z, Xiang Y, Kong L, et al. Hierarchical zeolites obtained by alkaline treatment for enhanced n-pentane catalytic cracking. Fuel 2022;313:122669.

[34] Bleken FL, Barbera K, Bonino F, Olsbye U, Lillerud KP, Bordiga S, et al. Catalyst deactivation by coke formation in microporous and desilicated zeolite H-ZSM-5 during the conversion of methanol to hydrocarbons. J Catal 2013;307:62–73.

[35] Han Z, Zhou F, Zhao J, Liu Y, Ma H, Wu G. Synthesis of hierarchical GaZSM-5 zeolites by a post-treatment method and their catalytic conversion of methanol to olefins. Microporous Mesoporous Mater 2020;302:110194. https://doi.org/10.1016/j.micromeso.2020.110194.

[36] Gackowski M, Tarach K, Kuterasiński Ł, Podobiński J, Jarczewski S, Kuśtrowski P, et al. Hierarchical zeolites Y obtained by desilication: porosity, acidity and catalytic properties. Microporous Mesoporous Mater 2018;263:282–8.

[37] Chen F, Zhang D, Shi L, Wang Y, Xu G. Optimized pore structures of hierarchical HY zeolites for highly selective production of methyl methoxyacetate. Catalysts 2019;9:865. https://doi.org/10.3390/catal9100865.

[38] Lv P, Yan L, Liu Y, Wang M, Bao W, Li F. Catalytic conversion of coal pyrolysis vapors to light aromatics over hierarchical Y-type zeolites. J Energy Inst 2020;93: 1354–63. https://doi.org/10.1016/j.joei.2019.12.005.

[39] Munir D, Amer H, Aslam R, Bououdina M, Usman MR. Composite zeolite beta catalysts for catalytic hydrocracking of plastic waste to liquid fuels. Mater Renew Sustain Energy 2020;9:1–13. https://doi.org/10.1007/s40243-020-00169-3.

[40] Munir D, Usman MR. Mesoporous HZSM-5 catalysts for the conversion of waste plastics to liquid fuels. J Porous Mater 2022;1:1–12. https://doi.org/10.1007/s10934-022-01212-6.

[41] Groen JC, Peffer LAA, Moulijn JA, Pérez-Ramírez J. Mesoporosity development in ZSM-5 zeolite upon optimized desilication conditions in alkaline medium. Colloids Surfaces A Physicochem Eng Asp 2004;241:53–8. https://doi.org/10.1016/j.colsurfa.2004.04.012.

[42] Groen JC, Moulijn JA, Pérez-Ramírez J. Alkaline posttreatment of MFI zeolites. From accelerated screening to scale-up. Ind Eng Chem Res 2007;46:4193–201. https://doi.org/10.1021/ie061146v.

[43] Gutiérrez A, Arandes JM, Castaño P, Olazar M, Bilbao J. Preliminary studies on fuel production through LCO hydrocracking on noble-metal supported catalysts. Fuel 2012;94:504–15. https://doi.org/10.1016/j.fuel.2011.10.010.

[44] Gutiérrez A, Arandes JM, Castaño P, Olazar M, Bilbao J. Enhancement of aromatic hydro-upgrading on a Pt catalyst by promotion with Pd and shape-selective supports. Fuel Process Technol 2012;101. https://doi.org/10.1016/j.fuproc.2012.03.014.

[45] Gutiérrez A, Arandes JM, Castaño P, Olazar M, Barona A, Bilbao J. Effect of space velocity on the hydrocracking of Light Cycle Oil over a Pt-Pd/HY zeolite catalyst. Fuel Process Technol 2012;95:8–15. https://doi.org/10.1016/j.fuproc.2011.11.003.

[46] Angeles MJ, Leyva C, Ancheyta J, Ramírez J. A review of experimental procedures for heavy oil hydrocracking with dispersed catalyst. Catal Today 2014;220–222: 274–94. https://doi.org/10.1016/j.cattod.2013.08.016.

[47] Trueba D, Palos R, Bilbao J, Arandes JM, Gutiérrez A. Product composition and coke deposition in the hydrocracking of polystyrene blended with vacuum gasoil. Fuel Process Technol 2021;224:107010. https://doi.org/10.1016/j.fuproc.2021.107010.

[48] Al-Attas TA, Zahir MH, Ali SA, Al-Bogami SA, Malaibari Z, Razzak SA, et al. Novel (Co-, Ni)-p-tert-butylcalix[4]arenes as dispersed catalysts for heavy oil upgrading: synthesis, characterization, and performance evaluation. Energy Fuels 2019;33: 561–73. https://doi.org/10.1021/acs.energyfuels.8b03619.

[49] Li Y, Liu S, Zhang Z, Xie S, Zhu X, Xu L. Aromatization and isomerization of 1-hexene over alkali-treated HZSM-5 zeolites: improved reaction stability. Appl Catal A Gen 2008;338:100–13. https://doi.org/10.1016/j.apcata.2007.12.026.

[50] Epelde E, Santos JI, Florian P, Aguayo AT, Gayubo AG, Bilbao J, et al. Controlling coke deactivation and cracking selectivity of MFI zeolite by H_3PO_4 or KOH modification. Appl Catal A Gen 2015;505:105–15. https://doi.org/10.1016/j.apcata.2015.07.022.

[51] Qin Z, Shen B, Gao X, Lin F, Wang B, Xu C. Mesoporous y zeolite with homogeneous aluminum distribution obtained by sequential desilication-dealumination and its performance in the catalytic cracking of cumene and 1,3,5-triisopropylbenzene. J Catal 2011;278:266–75. https://doi.org/10.1016/j.jcat.2010.12.013.

[52] Gil B, Mokrzycki Ł, Sulikowski B, Olejniczak Z, Walas S. Desilication of ZSM-5 and ZSM-12 zeolites: impact on textural, acidic and catalytic properties. Catal Today 2010;152:24–32. https://doi.org/10.1016/j.cattod.2010.01.059.

[53] Gayubo AG, Alonso A, Valle B, Aguayo AT, Bilbao J. Selective production of olefins from bioethanol on HZSM-5 zeolite catalysts treated with NaOH. Appl Catal B Environ 2010;97:299–306. https://doi.org/10.1016/j.apcatb.2010.04.021.

[54] Feliczak-Guzik A. Hierarchical zeolites: Synthesis and catalytic properties. Microporous Mesoporous Mater 2018;259:33–45. https://doi.org/10.1016/j.micromeso.2017.09.030.

[55] Umar M, Abdulazeez I, Tanimu A, Ganiyu SA, Alhooshani K. Modification of ZSM-5 mesoporosity and application as catalyst support in hydrodesulfurization of dibenzothiophene: Experimental and DFT studies. J Environ Chem Eng 2021;9: 106738. https://doi.org/10.1016/j.jece.2021.106738.

[56] Tarach K, Góra-Marek K, Tekla J, Brylewska K, Datka J, Mlekodaj K, et al. Catalytic cracking performance of alkaline-treated zeolite Beta in the terms of acid sites properties and their accessibility. J Catal 2014;312:46–57. https://doi.org/10.1016/j.jcat.2014.01.009.

[57] Weitkamp J. Catalytic hydrocracking-mechanisms and versatility of the process. ChemCatChem 2012;4:292–306. https://doi.org/10.1002/cctc.201100315.

[58] Becker PJ, Serrand N, Celse B, Guillaume D, Dulot H. A single events microkinetic model for hydrocracking of vacuum gas oil. Comput Chem Eng 2017;98:70–9. https://doi.org/10.1016/j.compchemeng.2016.11.035.

[59] Shabtai J, Xiao X, Zmierczak W. Depolymerization–liquefaction of plastics and rubbers. 1. Polyethylene, polypropylene, and polybutadiene. Energy Fuels 1997; 11:76–87. https://doi.org/10.1021/EF960076+.

[60] de Jong KP, Zečević J, Friedrich H, de Jongh PE, Bulut M, van Donk S, et al. Zeolite Y crystals with trimodal porosity as ideal hydrocracking catalysts. Angew Chem 2010;122:10272–6. https://doi.org/10.1002/ange.201004360.

[61] Li J, Li X, Zhou G, Wang W, Wang C, Komarneni S, et al. Catalytic fast pyrolysis of biomass with mesoporous ZSM-5 zeolites prepared by desilication with NaOH solutions. Appl Catal A Gen 2014;470:115–22. https://doi.org/10.1016/j.apcata.2013.10.040.

[62] Milato JV, França RJ, Rocha AS, Calderari MRCM. Catalytic co-pyrolysis of oil sludge with HDPE to obtain paraffinic products over HUSY zeolites prepared by dealumination and desilication. J Anal Appl Pyrolysis 2020;151:104928. https://doi.org/10.1016/j.jaap.2020.104928.

[63] Quitian A, Fernández Y, Ancheyta J. Viscosity reduction of heavy oil during slurry-phase hydrocracking. Chem Eng Technol 2019;42:148–55. https://doi.org/10.1002/ceat.201800102.

[64] Nguyen MT, Nguyen NT, Cho J, Park C, Park S, Jung J, et al. A review on the oil-soluble dispersed catalyst for slurry-phase hydrocracking of heavy oil. J Ind Eng Chem 2016;43:1–12. https://doi.org/10.1016/j.jiec.2016.07.057.

[65] Karakhanov E, Maximov A, Kardasheva Y, Vinnikova M, Kulikov L. Hydrotreating of light cycle oil over supported on porous aromatic framework catalysts. Catalysts 2018;8:397–411. https://doi.org/10.3390/catal8090310.3390/catal809039797.

[66] Gumming KA, Wojciechowski BW. Hydrogen transfer, coke formation, and catalyst decay and their role in the chain mechanism of catalytic cracking. Catal Rev 1996; 38:101–57. https://doi.org/10.1080/01614949608006455.

[67] Anderson PC, Sharkey JM, Walsh RP. Calculation of the research octane number of motor gasolines from gas chromatographic data and a Nerw approach to motor gasoline quality control. J Inst Pet 1972;58:83–94.

[68] Escola JM, Aguado J, Serrano DP, Briones L, Díaz De Tuesta JL, Calvo R, et al. Conversion of polyethylene into transportation fuels by the combination of thermal cracking and catalytic hydroreforming over Ni-supported hierarchical beta zeolite. Energy Fuels 2012;26:3187–95. https://doi.org/10.1021/ef300938r.

[69] Ochoa A, Valle B, Resasco DE, Bilbao J, Gayubo AG, Castaño P. Temperature programmed oxidation coupled with in situ techniques reveal the nature and location of coke deposited on a Ni/La2O3-αAl2O3 catalyst in the steam reforming of bio-oil. ChemCatChem 2018;10:2311–21. https://doi.org/10.1002/cctc.201701942.

[70] Ibáñez M, Pérez-Uriarte P, Sánchez-Contador M, Cordero-Lanzac T, Aguayo AT, Bilbao J, et al. Nature and location of carbonaceous species in a composite HZSM-5 zeolite catalyst during the conversion of dimethyl ether into light olefins. Catalysts 2017;7:254. https://doi.org/10.3390/catal7090254.

[71] Cordero-Lanzac T, Ateka A, Pérez-Uriarte P, Castaño P, Aguayo AT, Bilbao J. Insight into the deactivation and regeneration of HZSM-5 zeolite catalysts in the conversion of dimethyl ether to olefins. Ind Eng Chem Res 2018;57:13689–702. https://doi.org/10.1021/acs.iecr.8B03308.

[72] Palos R, Rodríguez E, Gutiérrez A, Bilbao J, Arandes JM. Kinetic modeling for the catalytic cracking of tires pyrolysis oil. Fuel 2022;309:122055. https://doi.org/10.1016/j.fuel.2021.122055.